Applied Physics A (2023) 129:874
https://doi.org/10.1007/s00339-023-07146-3

Applied Physics A
Materials Science & Processing

Efficiency improvement of commercial silicon solar cells using bilayers of luminescent nanomaterials

A. Cordova-Rubio[1,2] · R. Lopez-Delgado[2,3] · A. Zazueta-Raynaud[2,4] · A. Ayon[1] · M. E. Alvarez-Ramos[2]

Received: 12 April 2023 / Accepted: 8 November 2023 / Published online: 30 November 2023
© The Author(s), under exclusive licence to Springer-Verlag GmbH, DE part of Springer Nature 2023

Abstract

Photoluminescent down-shifting Silicon (Si) and Zinc Oxide (ZnO) Quantum Dots (QDs) were synthesized and employed in spectral converter layers to increase the photovoltaic performance of commercial solar cells. Poly-methyl-methacrylate (PMMA) was used as a matrix host to provide a transparent support for the quantum dots. The thickness of the photoluminescent QD layers and the particle concentration in the polymer were optimized to reduce reflectivity and increase the power generation. Different luminescent films' configurations were tested on fully functional solar cells, including single type of QD (Si or ZnO) layer and double layer of QDs (Si + ZnO). The colloidal QDs presented optical bandgaps of 2.97 eV and 3.40 eV for the Si QDS and ZnO QDs, respectively, difference that was advantageous for a double-layer configuration. The absorption of both Si QDS and ZnO QDs was mainly in the UV region, while their luminescence consisted of broad bands centered at 525 nm and 545 nm, respectively, providing an attractive stokes shift to be employed as spectral converter layer. The combination of UV absorption, downshifted emission, and reflectivity reduction by the QD-based layers produced improvements in the power conversion efficiencies of commercial silicon solar cells from 14.42 to 15.36%, which represent an overall improvement of ~ 6.5%. The collected results represent a promising strategy to improve the photovoltaic performance of new and existing devices.

Keywords Quantum dots · Solar cell · Photovoltaic · Power conversion efficiency

1 Introduction

Nowadays, commercial photovoltaic panels mainly consist of silicon-based solar cells, since their efficiencies are costly effective [1, 2]. However, since the most effective spectral response of silicon-based solar cells lies in the range from 500 to 900 nm, a considerable portion of the solar spectrum is not well collected. This shortcoming could be compensated by the employment of photoluminescent materials that exhibit a Stokes shift [3, 4], as a method to extend the spectral response of a complete device, by absorbing photons in the high energy region and re-emitting in a lower energy range, where silicon solar cells exhibit a better response. Quantum dots (QDs) are semiconductor nanostructures that confine the charge carriers to a nanoscale providing a spectral difference between their optical absorption and luminescent emission, making them excellent candidates to be employed as spectral converters [5–7]. Zinc oxide (ZnO) is a semiconductor that has been studied and applied in many areas due to its wide bandgap of 3.3 eV and its optical and electrical properties [8, 9]. It has been successfully demonstrated that it is possible to obtain zinc oxide nanostructures from a variety of methods, such as thermal evaporation [10], microwaves [11], sol–gel [12], wet chemicals [13], etc. Typically, zinc oxide quantum dots (ZnO QDs) exhibit luminescent emissions in the yellow–green region of the electromagnetic spectrum due to different contributions caused by intrinsic defects that can be attributed to bulk or surface

✉ A. Cordova-Rubio
ale.cordovar@gmail.com

[1] Department of Physics and Astronomy, University of Texas at San Antonio, MEMS Research Lab, One UTSA Circle, San Antonio, TX 78249, USA

[2] Departamento de Física, Universidad de Sonora, Blvd. Luis Encinas y Rosales, Col. Centro, 83000 Hermosillo, SON, México

[3] Investigadores por México-CONAHCYT-Universidad de Sonora, Luis Encinas y Rosales S/N, 83000 Hermosillo, SON, México

[4] Universidad Estatal de Sonora, Av. Ley Federal del Trabajo S/N, 83100 Hermosillo, SON, México

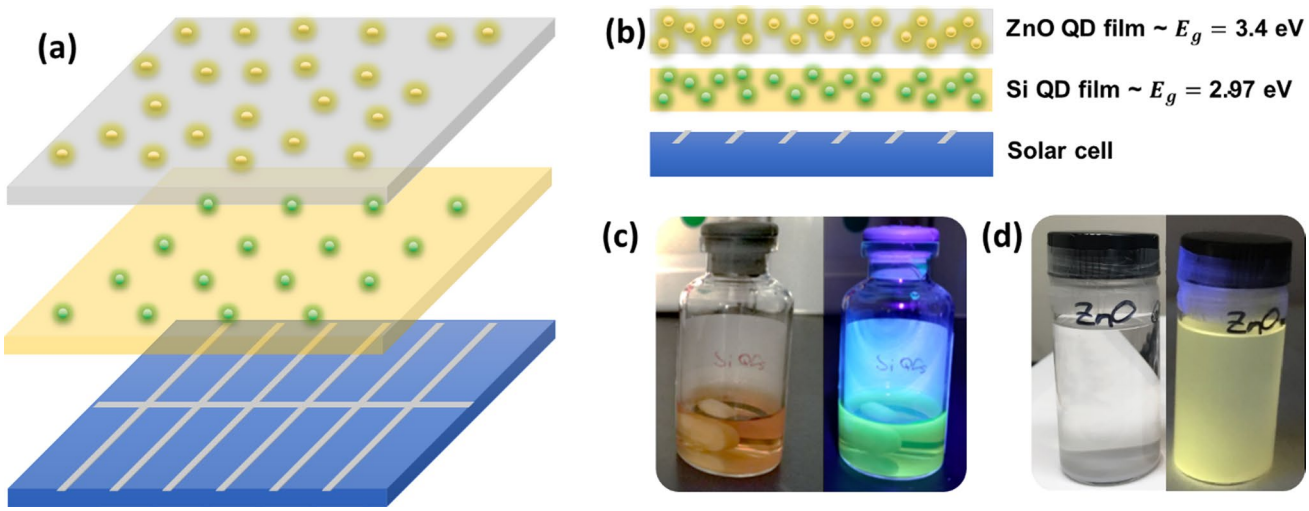

Fig. 1 **a** Schematic representation of a photovoltaic device with Si QDs layer + ZnO QDs layer. **b** Cross-section view of device structure and images of colloidal QDs solutions under visible and UV light of **c** Si QDs and **d** ZnO QDs' samples

defects [14]. Silicon (Si) is a material in the semiconductor family that is inert, abundant, economical, and non-toxic. Si QDs also exhibit effective visible emission due to adequate surface modification that favors radiative recombination and the quantum confinement effect [15]. Different synthesis methods have been studied and described so far, including ultrasonic dispersion of electrochemically etched silicon [16], laser-driven silane pyrolysis [17, 18], gas phase synthesis [19, 20], microemulsion synthesis [15], supercritical fluid synthesis [21], and wet chemistry techniques such as salt reduction in inert organic solvents [22, 23] and in micelles using sodium hydride reagents [19, 20, 24]. Strong quantum confinement in silicon increases the probability of radiative recombination through the direct band-to-band transitions and reduces indirect phonon-assisted transitions [25]. Photoluminescent Si and ZnO QDs present optical properties that make them promising candidates for the development of optoelectronic devices, such as application in solar cells to increase their energy conversion efficiency [19, 26]. A promising approach to enhance the photovoltaic performance of solar cells consists of the deployment of luminescent films as multilayer "tandem-like" structures with different bandgaps [27–29]. Here, the individual films are designed to target specific photon energies while letting photons with energies below its bandgap to interact with the next film, which subsequently does a similar process letting the lower energy photons to be absorbed by the solar cell.

In this work, we report the synthesis and characterization of Si and ZnO QDs and their employment as tandem-like bilayer spectral converters on photovoltaic devices. Figure 1 shows the proposed method to improve the performance of commercial solar cells, exploiting the band-gap differences of ZnO and Si quantum dots. With the bilayer spectral conversion process, it is possible to decrease the energy losses of silicon solar cells and contribute to an increase in power conversion efficiency. Ostensibly, the presence of films with quantum dots increases the photovoltaic performance, particularly in the high energy range. The deployment of the aforementioned bilayer with a down-shifting effect on solar cells showed that the observed results could be crucial in the proliferation of photovoltaic structures, which holds promise for applying this same strategy employing coatings of different quantum dots.

2 Experimental details

2.1 Characterization methods

Photoluminescent effects of the synthesized QDs were collected with an Ocean Optics Flame-S-UV–Vis spectrometer. The UV/Vis absorption spectra were collected with a Cary 5000 UV–Vis–NIR spectrometer. X-ray diffractometry was characterized with a Rigaku Ultima IV using K-Alpha1 radiation with a wavelength of 1.54 Å. The transmission electron microscopy images (TEM) were obtained with a JEOL 2010-F electron microscope with an operating voltage of 200 kV. The gravimetric measurement of the concentration of the QDs was performed using a quartz crystal microbalance (QCM) Model QCM200, Stanford Research Systems Inc, operating at room temperature and atmospheric pressure in a clean room environment. The thickness of the deposited films was measured using an ellipsometer J. A. Woollam V-vase. The current–voltage performance of the solar cells was collected under an AM1.5G illumination employing a solar simulator Oriel Sol2A at standard testing

conditions, i.e., 1000 W/m^2 at room temperature. The external quantum efficiency (EQE) was also performed with a Newport External Quantum Efficiency Measurement System (QEPVSI-B).

2.2 Synthesis of silicon quantum dots

Silicon QDs were synthesized employing a water-based colloidal approach [30, 31]. To this end, two precursor solutions were prepared; in the initial solution, 2.0 mL of 3-aminopropyl triethoxysilane ($H_2N(CH_2)_3Si(OC_2H_5)_3$ 99%, Sigma-Aldrich) (APTES) was added to 4 mL of de-ionized water (DI water) and stirred for 10 min. Next, a 0.1 M of sodium (+)-L-ascorbate ($C_6H_7NaO_6$) ≥ 98% (SA) second solution was prepared by dissolving 0.1819 g of SA to 10 ml of de-ionized water. Subsequently, 1.25 ml of the SA solution was mixed with the APTES solution and stirred for 30 min. It has been reported that a silica/silicate matrix host is obtained besides the nanoparticle formation and can be employed directly as the Si QDs support [32]. The obtained QDs were deployed in solar cells as synthesized.

2.3 Synthesis of ZnO quantum dots

ZnO quantum dots were produced from a controlled precipitation synthesis method at room temperature [14, 33]. An initial 0.02 M zinc acetate solution was prepared by dissolving 0.256 g of zinc acetate ($C_4H_6O_4Zn$ 99.99%, Sigma-Aldrich) in 70 mL of absolute ethanol. A second solution of 0.1 M lithium hydroxide was prepared by dissolving 0.125 g of LiOH (≥ 98% Sigma-Aldrich) in 30 mL of absolute ethanol. Once both solutions were perfectly dissolved, the LiOH solution was slowly poured into the zinc acetate solution under constant magnetic stirring. The pH was constantly monitored and the LiOH solution was poured until a pH value of 10 was obtained. Then, the zinc acetate–LiOH mixed solution was placed in an ultrasonic bath for 3 h to create the ZnO QDs. To promote the precipitation and collection of ZnO QDs, hexane was added to the colloidal solution with a volumetric ratio of 3:1 and left at room temperature for 24 h [33]. Once the QDs precipitated, the supernatant was removed, and the ZnO QDs were washed by centrifugation and redispersed in absolute ethanol.

2.4 Quantum dot concentration determination

To determine the QDs' concentration, a gravimetric method was employed. This method consists of depositing droplets of known volume on a quartz crystal with a characteristic oscillation frequency [34]. An increase of mass on the quartz crystal surface causes the oscillation frequency to decrease, which was produced by droplet deposition. In the case of pure ethanol (QCM calibration), as the solvent evaporates, the oscillation frequency returns to its initial value, indicating that no mass is remaining on the surface of the crystal. Once the QCM calibration is confirmed, droplets of 20 µL containing ZnO QDs in ethanol were deposited on the quartz crystal and the solvent was allowed to evaporate, leaving the quantum dots on the quartz crystal and modifying its oscillation frequency. Finally, according to Sauerbrey equation $\Delta f = -C_f \Delta m$ [35], where C_f is the sensitivity factor of the crystal (56.6Hz^{-1}cm^2), a change in the observed frequency Δf (Hz), leads to a change in mass per unit area Δm (µg/cm^2), allowing the calculation of the deposited ZnO QDs mass.

2.5 Quantum dots' deployment on solar cells

The analysis of the influence of the QDs on solar cells was carried out by incorporating a first layer of Si QDs and a subsequent layer of ZnO QDs on fully functional photovoltaic devices (Fig. 1b). As it was mentioned, the Si QDs' film was obtained by the deposition of the as synthesized Si QDs' solution. On the other hand, to deploy the ZnO nanostructures on the solar cells, polymethyl methacrylate (PMMA) was employed as matrix host due to its resistance to ultraviolet light and transparency [36]. Different concentrations of ZnO QDs in the PMMA films were produced as follows: (i) 0.5 ml of ZnO QDs in ethanol were centrifuged to promote the precipitation of the particles, (ii) the solvent was removed, leaving the QDs at the bottom, and (iii) the QDs were dispersed in 0.5 ml, 1 ml, and 1.5 ml of PMMA (495 PMMA A2, Microchem). The films were obtained by spin coating on the window surface of all solar cells. According to the numerical analysis of Dyakov [37], the thicknesses of both Si and ZnO QDs layers were optimized to 140 nm and 60 nm, respectively, to reduce the reflection related losses. To achieve the desired thickness of the different layers, Si QDs were deposited at 5,000 rpm, while the different concentrations of ZnO QDs/PMMA were deployed at 4,000 rpm. The thicknesses of both layers were corroborated by ellipsometry measurements. To determine the influence of Si and ZnO QDs on the efficiency of solar cells, commercial polycrystalline silicon devices with dimensions of 52 mm × 38 mm and a thickness of 200 µm were employed. The solar cells were characterized before and after the incorporation of each film to determine their influence on the PCE of the photovoltaic devices.

3 Results and discussion

3.1 Structural and size determination

The crystal structure of the ZnO QDs was determined from the XRD patterns shown in Fig. 2a. According to the

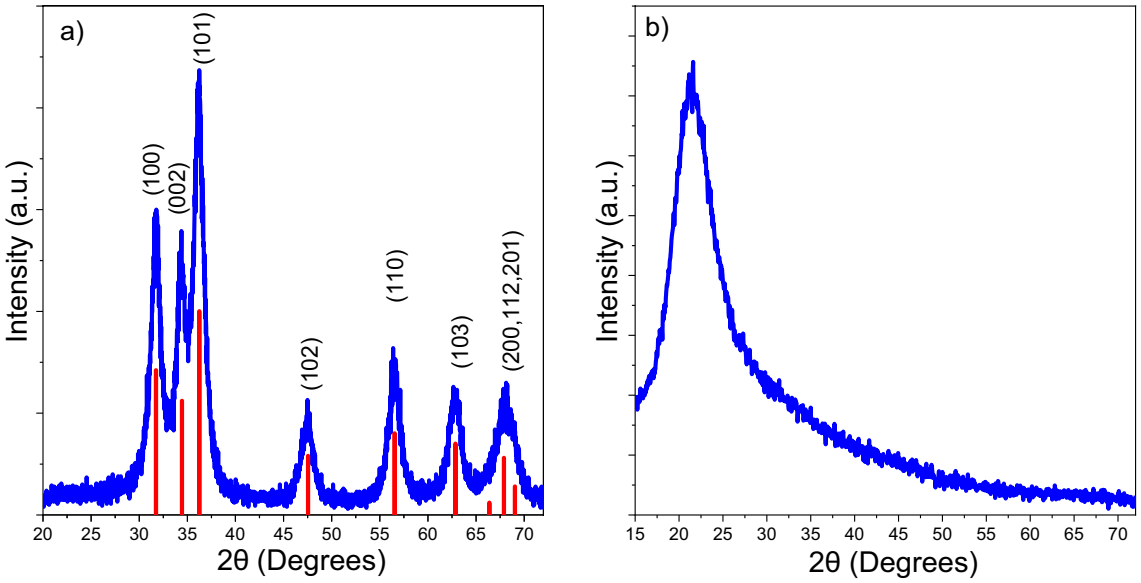

Fig. 2 X-ray diffraction pattern of **a** ZnO QDs with the crystallographic card (00-001-1136) and **b** Si QDs embedded in a silica-based matrix

crystallographic card (00-001-1136) [38], the ZnO QDs' crystal structure was identified as hexagonal wurtzite. This structure is characterized by three prominent diffraction peaks located at 31.73°, 34.45°, and 36.27° corresponding to the crystalline planes 100, 002, and 101, respectively. Also, the 102, 110, and 103 planes were located at 47.51°, 56.52°, and 63.89°, respectively. Finally, a broad peak centered at 68.25° was formed by the three contributions associated with planes 200, 112, and 201 at 66.34°, 67.86°, and 69.07°, respectively. This observation is consistent with the previous reports found elsewhere [39], indicating that binary composite semiconductors in the group II–VI crystallize either in blende of cubic zinc or hexagonal wurtzite structure (Wz). The XRD characterization of Si QDs was also performed; however, since the Si QDs were employed as synthesized, the precursor subproducts provided a silica-based matrix to self-contain the QDs [32]. In accordance with this, the XRD patterns reveal only the signal of the amorphous silica-based matrix and not the crystalline structure of QDs, as shown in Fig. 2b [40].

The X-ray diffractogram data were employed to calculate the crystallite sizes by analyzing the preferential peaks and applying the Scherrer equation [41]

$$D = \frac{K\lambda}{\beta \cos\theta}, \tag{1}$$

where D is the crystallite size, K is a dimensionless shape factor (0.9), λ is the wavelength of the radiation, θ is the position of the peak, and β is the peak's full width at half maximum (FWHM). *A* deconvolution of peaks for spherical particles was employed to obtain the positions (θ) and breadths (β) [42, 43]. The calculated ZnO crystallite size employing Scherrer equation was ~ 5.2 nm.

Transmission electron microscopy analysis was performed to analyze the size distribution of the synthesized ZnO and Si QDs. As may be seen in Fig. 3, ZnO QDs presented an averaged diameter of 5.1 nm, while the Si QDs were slightly smaller with diameters of 3.6 nm. Also, it was possible to calculate the size of the QDs employing the optical bandgap considering the quantum confinement of the particles using the Brus' equation [44]

$$E_g^{\mathrm{QD}} \cong E_g^{\mathrm{bulk}} + \frac{\hbar^2\pi^2}{2R^2}\left(\frac{1}{m_{e*}} + \frac{1}{m_{h*}}\right) - \frac{1.8e^2}{4\pi \in\in_0 R}, \tag{2}$$

where $\hbar$ is Planck's constant, E_g^{bulk} is the bulk band-gap energy, R is the radius of the QDs, m_{e*} is the effective mass of the holes, and m_{e*} is the effective mass of the electrons [45]. Using Eq. (2) and the band-gap results obtained from the Tauc's graphic method, we found that the approximate sizes were 5.8 nm for ZnO QDs and 3.76 nm for Si QD. The sizes calculated with the methods described above are reported in Table 1.

3.2 Optical characterization

The optical characterization of the quantum dots included the absorption and photoluminescent spectra measured from 275 to 850 nm. Also, a calculation of their energy bandgap was obtained. In the ZnO QDs case, the spectrum presented an abrupt increase of absorption below 375 nm, while in the

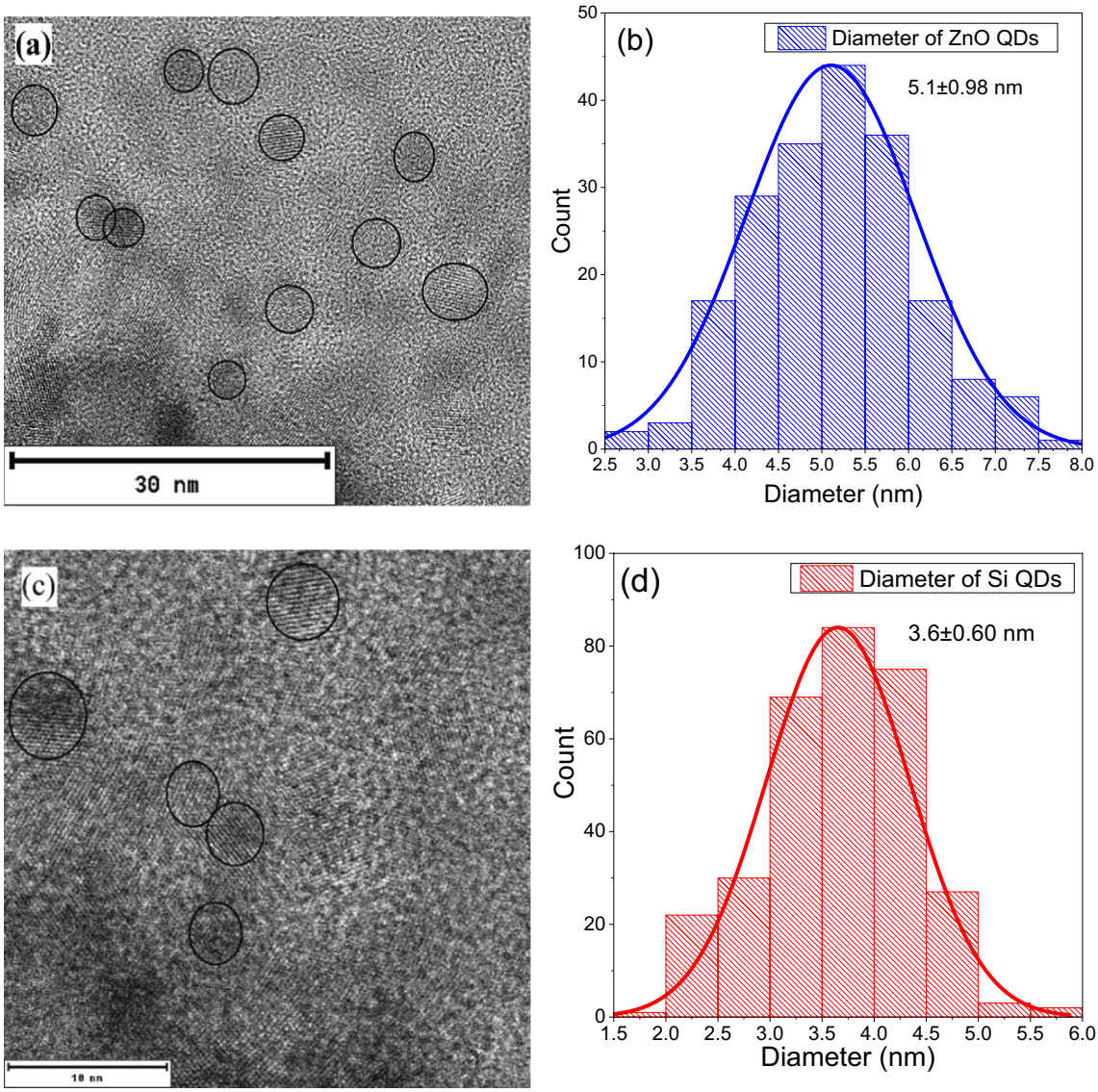

Fig. 3 **a** TEM image of ZnO QDs and **b** ZnO QDs' size distribution obtained from TEM analysis. **c** TEM image of Si QDs and **d** the histogram of the size distribution of Si QDs

Table 1 Size of the quantum dots employing different methods

	TEM (nm)	Brus equation (nm)
ZnO QDs	5.1 ± 0.62	5.80
Si QDs	3.6 ± 0.60	3.76

Si QDs' spectra, the increase was observed below 475 nm (Fig. 4). To obtain their photoluminescent characteristics, both materials were excited with wavelengths near to its absorption edge. As a result, the synthesized ZnO quantum dots exhibited a broad photoluminescent band centered at ~ 545 nm when excited with a wavelength of 350 nm [14], as shown in Fig. 4a, while Si QDs shown a photoluminescent band centered at ~ 525 nm when excited with a wavelength of 450 nm (see Fig. 4b, these values are consistent with previously reported works [30, 31]. To calculate the energy bandgap of the synthesized quantum dots, Tauc's plot graphic method (Eq. 3) was used [46]

$$B_1(Ah\nu)^m + E_g = h\nu, \tag{3}$$

where A is the measured absorbance, which is proportional to the absorption coefficient, B_1 is a constant, h is the Planck's constant, ν is the photon frequency, E_g is the band-gap energy, and m is a parameter related to the exciton

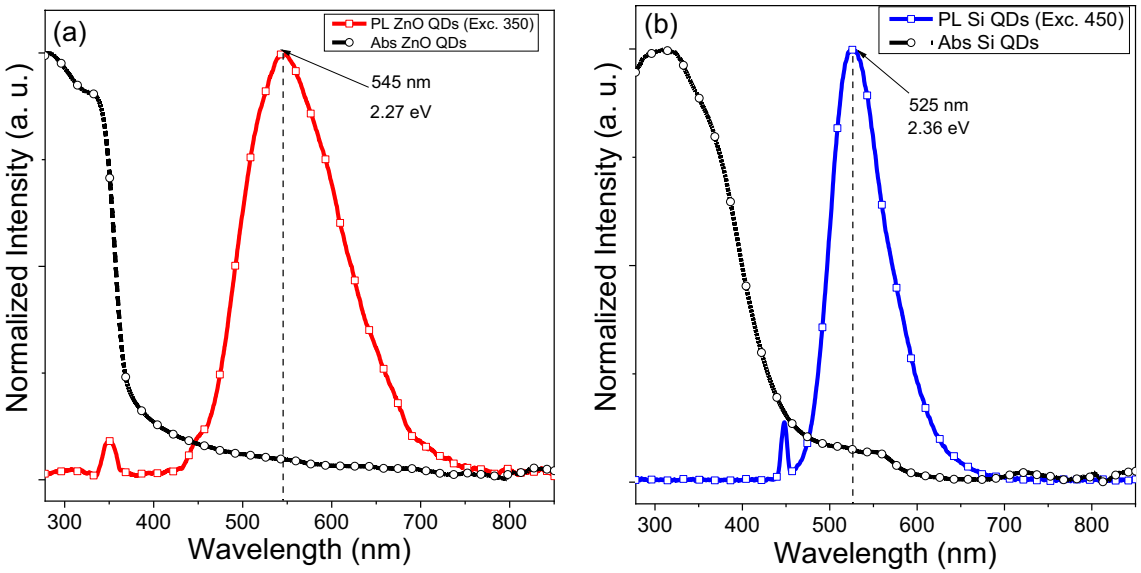

Fig. 4 Absorption (dashed line) and photoluminescence (continuous line) spectra characterization for **a** ZnO QDs with an excitation wavelength of 350 nm and **b** Si QDs with an excitation of 450 nm

transition with value of 2 corresponding to the direct allowed transition. By plotting $B_1(Ah\nu)^2$ vs. hν and considering a linear fit, we were able to obtain the values E_g of 3.40 eV for the ZnO QDs and 2.97 for the Si QDs, as shown in Fig. 5.

3.3 ZnO QDs' concentration

To measure the amount of ZnO QDs employed in the luminescent films, QCM measurements were performed to calculate the ZnO QDs' concentration. A variation in the resonant frequency was observed due to the residual mass of the ZnO QDs on the quartz crystal. A decrease of 127 ± 0.3 Hz in the resonant frequency was observed due to the presence of the QDs, indicative of a mass increase of 2.25 ± 0.005 μg/cm^2, as shown in blue in Fig. 6. With these observations, it was possible to calculate the total average mass of residual ZnO QDs. The mass concentration of ZnO nanoparticles c_m in a droplet of volume v is calculated from

$$c_m = \frac{\Delta m S}{v}, \tag{4}$$

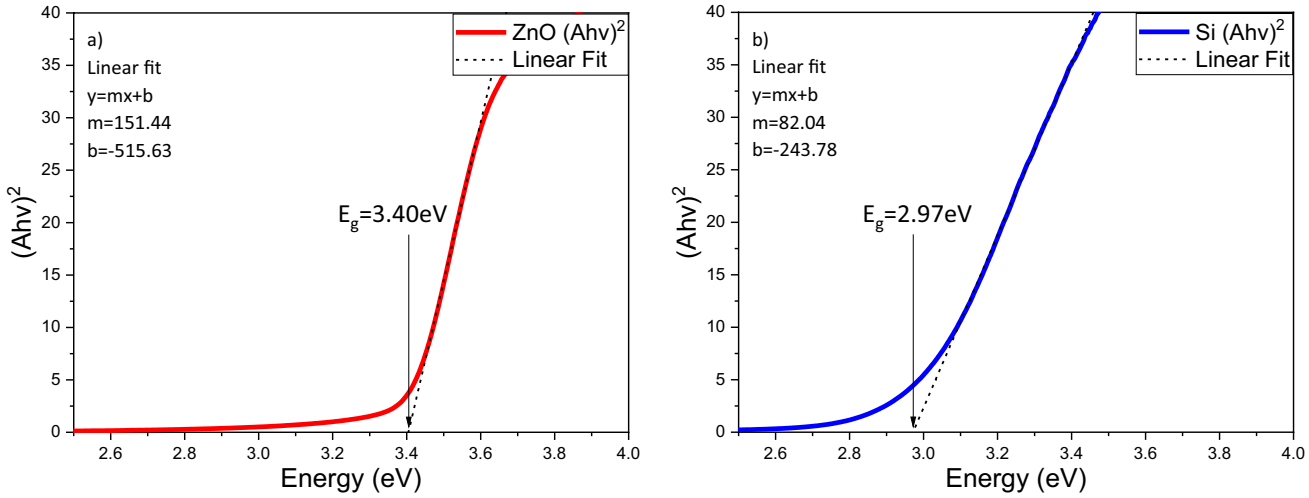

Fig. 5 **a** Graphic representation of Tauc's method $B_1(Ah\nu)^2$ vs $h\nu$ for **a** ZnO QDs. and **b** Si QDs

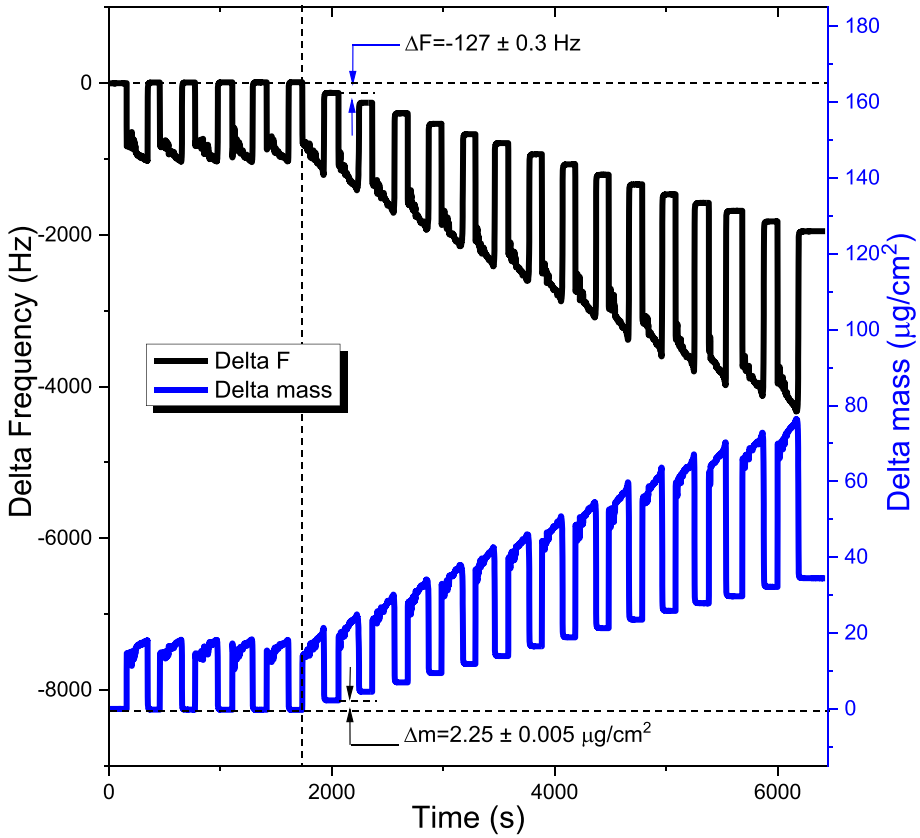

Fig.6 QCM and frequency trace recorded during the sequential injection of 20 μL drops of ZnO QDs and changes in the mass recorded by the sensor due to the presence of residual ZnO QDs

where S is the surface area of the quartz crystal ($S = 4.91$ cm^2) [35]. By knowing the volume of the deposited droplets (20 μL), it was possible to extract the mass concentration $c_m = 0.57 \pm 0.09 \frac{\mu g}{\mu L}$. According to this information and following the deposition procedure mentioned in Sect. 2.5, the ZnO films contained ~ 285 μg of QDs.

3.4 Solar cell characterization

To corroborate the influence of the luminescent films on the performance of functional silicon solar cells, two independent characterizations were performed: current–voltage (I–V) characteristics under solar simulated light and external quantum efficiency (EQE). As mentioned in the experimental section, silicon quantum dots were deposited as synthesized, while three different concentrations of ZnO were employed (dispersed in 0.5 ml, 1 ml, and 1.5 ml of PMMA). Figure 7 shows the I–V characterization and EQE of the solar cells before and after the coatings of Si and ZnO QDs, while Table 2 summarizes the average photovoltaic parameters measured before and after the deposition of each luminescent film. As can be seen in Table 2, it was found that the incorporation of the luminescent films improved the photocurrent generation, leading to increases from 35.49 to 35.78 mA/cm^2, from 35.43 to 35.65 mA/cm^2, and from 35.98 to 36.35 mA/cm^2 for the samples with quantum dots dispersed in 0.5 ml, 1 ml, and 1.5 ml of PMMA respectively. Also, it was observed that both the open circuit voltage (Voc) and fill factor (FF) were enhanced after the deposition of the films. Remarkably, the FF enhancement is thought to be related to a decrease of "high energy" photons reaching the solar cell surface, since it has been studied that photoluminescent down-shifting layers help to mitigate thermalization loses as well as surface recombination in solar cells [47–50]. In this sense, the results suggest that a possible prevention of increase in the device's surface temperature could have been produced in comparison to the uncoated device, and, according to previous reports about the influence of temperature and irradiance on the parameters of photovoltaic cells using both theoretical and experimental approaches, increases of temperature could affect directly the FF [51–55]. The combination of these results led to increases on the power conversion efficiencies of the photovoltaic devices from 14.93 to 15.54%, from 14.42 to 15.36%, and from 14.81 to 15.42% for the samples with quantum dots dispersed in 0.5 ml, 1 ml, and 1.5 ml of PMMA, which represents improvements of 4.09%, 6.52%, and 4.12% of the overall PCE, respectively. These results are promising, since the PCE enhancements for single layer have been found of 4.8% for ZnO QDs [14], 2.23% for chlorophyll-A [56], and 4.8% for ZnSe [57] on commercial silicon solar cells, while enhancements of

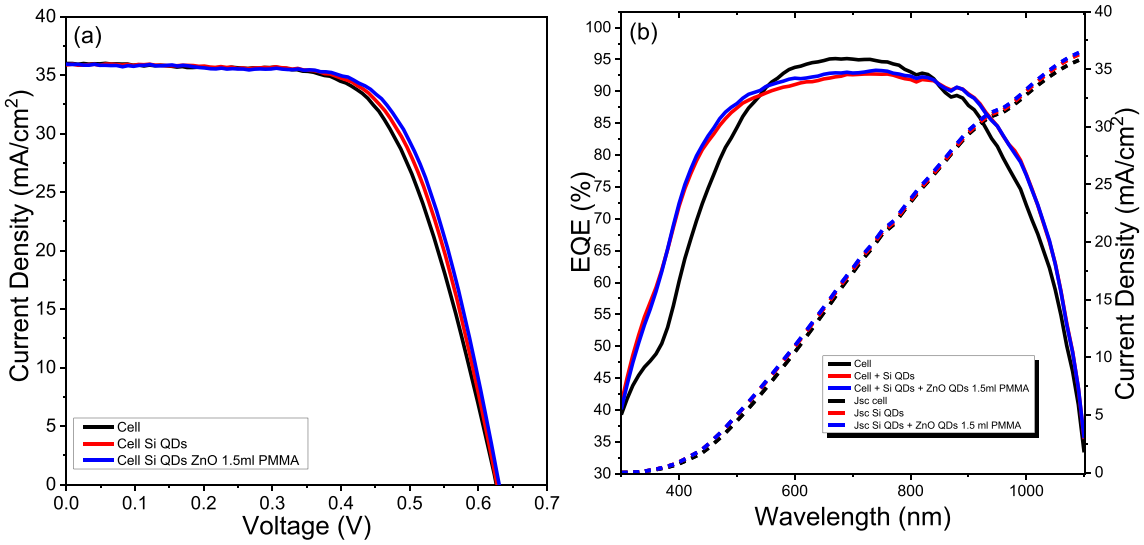

Fig. 7 **a** Current–Voltage characteristics. **b** Measured external quantum efficiency of solar cells before and after deploying layers of Si QDs and ZnO QDs (solid line). Calculated short-circuit current density from EQE data, according to Eq. 5 without QDs and with QDs (dashed line)

Table 2 Detailed J–V characteristics of the solar cells before and after deploying layers of Si QDs and different concentrations of ZnO QDs

	Bare SC	SC + Si	SC + Si + ZnO 0.5PMMA	Bare SC	SC + Si	SC + Si + ZnO 1.0PMMA	Bare SC	SC + Si	SC + Si + ZnO 1.5PMMA
V_{OC} (mV)	620.11	622.62	622.83	623.31	621.80	624.54	627.26	627.84	631
J_{SC} (mA/cm^2)	35.49	35.57	35.78	35.43	35.59	35.65	35.98	36.27	36.35
FF (%)	67.52	67.70	69.73	64.67	67.80	68.64	66.01	66.29	66.37
PCE (%)	14.93 ± 0.06	15.07 ± 0.1	15.54 ± 0.09	14.42 ± 0.19	15.01 ± 0.05	15.36 ± 0.07	14.81 ± 0.12	15.14 ± 0.18	15.42 ± 0.17
ΔPCE (%)		0.94	*4.09*		4.09	*6.52*		2.23	*4.12*

The figures highlighted in italics are the final results with two types of coatings. In this case there are 3 results, 3 concentrations of ZnO quantum dots on PMMA were used

0.81% and 0.61% were found for Si QDs deployed on silicon and perovskite solar cells, respectively [58]. External quantum efficiencies were analyzed to evaluate the effect of the incorporation of two luminescent down-shifting layers on the spectral response of silicon solar cells. As shown in Fig. 7, an increase in the spectral response of the solar cells in the short-wavelength range was observed due to the down-shifting effect compared to the uncoated cell. Analyzing the down-shifting effect region, an effective EQE increase of 9.86% and 10.20% is observed by depositing Si QD and ZnO QD, respectively. This improvement was calculated by comparing the EQE integral over the 300–550 nm wavelength range, i.e., where the QDs absorb photons. These results are comparable to those reported previously [59]. Nevertheless, a degradation of the EQE in the 550–870 nm region was presented, corresponding to an effective decrease of 2% when depositing the first coating compared to the initial efficiency (cell without QDs). This decrease shows a slight recovery after the second coating, obtaining only 1.41% below the initial value. Additionally, in the region of 870–1100, a slight increase of 4% is obtained with respect to the solar cell without QDs. These effects have been previously studied for different luminescent coatings, proposing that a variation of the quantum efficiency could be produced by the non-optimal refractive index of the luminescent coatings [48]. Different computational models have reported similar results based on the modification of the AM1.5G incident spectrum according to the absorption and emission properties of the luminescent layers [59–62]. Additionally, the data collected from the EQE measurements were also used to corroborate the results of the short-circuit current density (J_{sc}) obtained with I–V characterization under solar simulator. To this end, the J_{sc} was extracted from the EQE spectrum by the equation

$$J_{sc} = q \int b_s(E) EQE(E) dE, \tag{5}$$

where q is the charge of the electron and $b_s(E)$ is the spectral flow density of incident photons. In all cases, the calculated

J_{sc} values corroborate the confidence of the reported solar cell performance herein.

4 Conclusions

ZnO and Si QDs were synthesized by straight forward and attractive methods. The obtained nanostructures have sizes of approximately 5.1 and 3.6 nm, respectively, presenting quantum confinement properties that modified their bulk band-gap values and allowing to use them as a tandem-like bilayer luminescent structure. The absorption and emission properties found on these materials are favorable for optimizing the operation of photovoltaic devices by deploying them over the solar cell´s window, since the individual films are designed to target specific photon energies, while letting photons with energies below its bandgap to interact with the next film, which subsequently does a similar process letting the lower energy photons to be absorbed by the solar cell. The collected data indicate that upon the deployment of the first coating of Si QDs, the solar cells exhibited increases in the main parameters of the devices, leading to a maximum increase of 4.09% in the PCE for the sample with the film with 1.0 ml PMMA. Upon deploying the second coating of PMMA with the dispersed ZnO QDs, the observed PCE improvement was 6.5%. We anticipate the observed results could prove crucial in the proliferation of photovoltaic structures.

Acknowledgements The authors would like to acknowledge the U.S. Army Research Office (Grant W911NF-13-1-0110), NSF (Grant 1650571), CONACYT, the Department of Physics and Astronomy at the University of Texas at San Antonio, and the Physics Department of the University of Sonora, for the financial support provided for this research project. The preliminary findings of our research project have been presented at the following international conferences: the Design, Test, Integration & Packaging of MEMS/MOEMS conference, the Microscopy & Microanalysis Meeting, and the International Materials Research Congress. These conferences provided a valuable platform for us to showcase our progress and receive feedback from experts in the field. The authors are grateful for the opportunity to share our work with such a knowledgeable and engaged audience and look forward to continuing to develop and refine our findings.

Author contributions All authors contributed to the conception and design of the study. Material preparation, data collection, and analysis were performed by ACR. The first draft of the manuscript was written by ACR. All authors read and approved the final manuscript and commented on previous versions of the manuscript. RLD and AZR reviewed the correct redaction and analysis of results. Financial support was provided by the U.S. Army Research Office and managed by AAA. This research project was supervised by EAR and AAA.

Funding This work was supported by CONACYT, the US Army Research Office (Grant W911NF-13-1-0110), and NSF (Grant 1650571). A Cordova-Rubio, A Zazueta-Raynaud, and R López-Delgado have received research support from CONACYT.

Data availability The datasets generated during and/or analyzed during the current study are available from the corresponding author on reasonable request.

Declarations

Conflict of interest The authors have no conflicts of interest to declare that are relevant to the content of this article.

Ethical approval This work was mainly supported by the University of Sonora and the University of Texas at San Antonio with financial support from CONAHCYT and the U.S. Army Research Office. The research presented does not involve humans or animals. The authors have no conflicts of interest to declare that are relevant to the content of this article.

References

1. S. Sharma, K.K. Jain, A. Sharma, Solar cells: in research and applications—a review. Mater. Sci. Appl. **6**(12), 1145 (2015)
2. B.P. Singh, S.K. Goyal, P. Kumar, Solar PV cell materials and technologies: analyzing the recent developments. Mater. Today **43**, 2843–2849 (2021)
3. A. Polman, M. Knight, E.C. Garnett, B. Ehrler, W.C. Sinke, Photovoltaic materials: present efficiencies and future challenges. Science **352**(6283), aad4424 (2016)
4. K. Ranabhat, L. Patrikeev, A. Antal'evna-Revina, K. Andrianov, V. Lapshinsky, E. Sofronova, An introduction to solar cell technology. J. Appl. Eng. Sci. **14**(4), 481–491 (2016)
5. F.P. García de Arquer, D.V. Talapin, V.I. Klimov, Y. Arakawa, M. Bayer, E.H. Sargent, Semiconductor quantum dots: technological progress and future challenges. Science **373**(6555), eaaz8541 (2021)
6. V. Biju, T. Itoh, A. Anas, A. Sujith, M. Ishikawa, Semiconductor quantum dots and metal nanoparticles: syntheses, optical properties, and biological applications. Anal. Bioanal. Chem. **391**, 2469–2495 (2008)
7. S.K. Gupta, K. Sudarshan, R. Kadam, Optical nanomaterials with focus on rare earth doped oxide: a review. Mater. Today Commun. **27**, 102277 (2021)
8. W.A. Mohamed et al., Quantum dots synthetization and future prospect applications. Nanotechnol. Rev. **10**(1), 1926–1940 (2021)
9. K. James Singh et al., Recent advances in two-dimensional quantum dots and their applications. Nanomaterials **11**(6), 1549 (2021)
10. M. Zheng, L. Zhang, G. Li, W. Shen, Fabrication and optical properties of large-scale uniform zinc oxide nanowire arrays by one-step electrochemical deposition technique. Chem. Phys. Lett. **363**(1–2), 123–128 (2002)
11. S. Komarneni, M. Bruno, E. Mariani, Synthesis of ZnO with and without microwaves. Mater. Res. Bull. **35**(11), 1843–1847 (2000)
12. K.M. Koczkur, S. Mourdikoudis, L. Polavarapu, S.E. Skrabalak, Polyvinylpyrrolidone (PVP) in nanoparticle synthesis. Dalton Trans. **44**(41), 17883–17905 (2015)
13. Z. Yu, M.R. Kumar, D. Sun, L. Wang, R. Hong, Large scale production of hexagonal ZnO nanoparticles using PVP as a surfactant. Mater. Lett. **166**, 284–287 (2016)
14. A. Zazueta-Raynaud, R. Lopez-Delgado, J. Pelayo-Ceja, M. Alvarez-Ramos, A. Ayon, Utilization of down-shifting photoluminescent ZnO quantum dots on solar cells. Mater. Res. Express **4**(7), 076203 (2017)
15. D.S. English, L.E. Pell, Z. Yu, P.F. Barbara, B.A. Korgel, Size tunable visible luminescence from individual organic monolayer

stabilized silicon nanocrystal quantum dots. Nano Lett. **2**(7), 681–685 (2002)
16. G.Y. Sung et al., Physics and device structures of highly efficient silicon quantum dots based silicon nitride light-emitting diodes. IEEE J. Sel. Top. Quantum Electron. **12**(6), 1545–1555 (2006)
17. A. Das, P.T. Snee, Synthetic developments of nontoxic quantum dots. ChemPhysChem **17**(5), 598–617 (2016)
18. L. Jin, H. Zhao, Z.M. Wang, F. Rosei, Quantum dots-based photoelectrochemical hydrogen evolution from water splitting. Adv. Energy Mater. **11**(12), 2003233 (2021)
19. S. Chinnathambi, S. Chen, S. Ganesan, N. Hanagata, Silicon quantum dots for biological applications. Adv. Healthc. Mater. **3**(1), 10–29 (2014)
20. J. Wu, J. Dai, Y. Shao, Y. Sun, One-step synthesis of fluorescent silicon quantum dots (Si-QDs) and their application for cell imaging. RSC Adv. **5**(102), 83581–83587 (2015)
21. S. Guruvenket et al., Synthesis of silicon quantum dots using cyclohexasilane (Si 6 H 12). J. Mater. Chem. C **4**(35), 8206–8213 (2016)
22. S. Wang, C. Li, P. Yang, M. Ando, N. Murase, Silica encapsulation of highly luminescent hydrophobic quantum dots by two-step microemulsion method. Colloids Surf. A **395**, 24–31 (2012)
23. R. Koole et al., On the incorporation mechanism of hydrophobic quantum dots in silica spheres by a reverse microemulsion method. Chem. Mater. **20**(7), 2503–2512 (2008)
24. M.A. Mumin, K.F. Akhter, O.O. Oyeneye, W.Z. Xu, P.A. Charpentier, Supercritical fluid assisted dispersion of nano-silica encapsulated CdS/ZnS quantum dots in poly (ethylene-co-vinyl acetate) for solar harvesting films. ACS Appl. Nano Mater. **1**(7), 3186–3195 (2018)
25. J.D. Holmes, K.J. Ziegler, R.C. Doty, L.E. Pell, K.P. Johnston, B.A. Korgel, Highly luminescent silicon nanocrystals with discrete optical transitions. J. Am. Chem. Soc. **123**(16), 3743–3748 (2001)
26. A.B. Djurišić, X. Liu, Y.H. Leung, Zinc oxide films and nanomaterials for photovoltaic applications. Phys. Status Solidi (RRL) **8**(2), 123–132 (2014)
27. J.Y. Huang, Y. Wang, G.T. Fei, S.H. Xu, Z. Zeng, B. Wang, TiO2/ZnO double-layer broadband antireflective and down-shifting coatings for solar applications. Ceram. Int. **49**(7), 11091–11100 (2023)
28. Z. Hu, L. Zhao, W. Li, S. Wang, B. Dong, Ag nanoparticle-modified double-layer composite film based on P25/NaLuF4: Yb3+/Er3+ and flower TiO2 for highly efficient dye-sensitized solar cells. Appl. Surf. Sci. **491**, 286–293 (2019)
29. M.J. Lim, Y.N. Ko, Y.C. Kang, K.Y. Jung, Enhancement of light-harvesting efficiency of dye-sensitized solar cells via forming TiO 2 composite double layers with down/up converting phosphor dispersion. RSC Adv. **4**(20), 10039–10042 (2014)
30. J. Wang, D.-X. Ye, G.-H. Liang, J. Chang, J.-L. Kong, J.-Y. Chen, One-step synthesis of water-dispersible silicon nanoparticles and their use in fluorescence lifetime imaging of living cells. J. Mater. Chem. B **2**(27), 4338–4345 (2014)
31. R. Lopez-Delgado et al., Solar cell efficiency improvement employing down-shifting silicon quantum dots. Microsyst. Technol. **24**, 495–502 (2018)
32. B. Das, S.M. Hossain, A.K. Pramanick, A. Dey, M. Ray, One-pot synthesis of gel glass embedded with luminescent silicon nanoparticles. ACS Appl. Mater. Interfaces **11**(2), 2507–2515 (2018)
33. J. Rodrıguez-Paéz, A. Caballero, M. Villegas, C. Moure, P. Duran, J. Fernández, Controlled precipitation methods: formation mechanism of ZnO nanoparticles. J. Eur. Ceram. Soc. **21**(7), 925–930 (2001)
34. K.A. Marx, Quartz crystal microbalance: a useful tool for studying thin polymer films and complex biomolecular systems at the solution– surface interface. Biomacromol **4**(5), 1099–1120 (2003)
35. V. Reipa, G. Purdum, J. Choi, Measurement of nanoparticle concentration using quartz crystal microgravimetry. J. Phys. Chem. B **114**(49), 16112–16117 (2010)
36. H. Gordillo, I. Suárez, R. Abargues, P. Rodríguez-Cantó, S. Albert, J. Martínez-Pastor, Polymer/QDs nanocomposites for waveguiding applications. J. Nanomater. **2012**, 33–33 (2012)
37. S.A. Dyakov, V.A. Tolmachev, E.V. Astrova, S.G. Tikhodeev, V.Y. Timoshenko, T.S. Perova, Numerical methods for calculation of optical properties of layered structures. Int. Conf. Micro- Nano-Electron. **7521**, 140–149 (2010)
38. D. Sun, M. Wong, L. Sun, Y. Li, N. Miyatake, H.-J. Sue, Purification and stabilization of colloidal ZnO nanoparticles in methanol. J. Sol-Gel Sci. Technol. **43**, 237–243 (2007)
39. H. Morkoç, Ü. Özgür, *Zinc Oxide: Fundamentals, Materials and Device Technology* (John Wiley & Sons, 2008)
40. E.S. Pouya, H. Abolghasemi, H. Fatoorehchi, B. Rasem, S.J. Hashemi, Effect of dispersed hydrophilic silicon dioxide nanoparticles on batch adsorption of benzoic acid from aqueous solution using modified natural vermiculite: an equilibrium study. J. Appl. Res. Technol. **14**(5), 325–337 (2016)
41. A.K. Zak, W.A. Majid, M.E. Abrishami, R. Yousefi, X-ray analysis of ZnO nanoparticles by Williamson-Hall and size–strain plot methods. Solid State Sci. **13**(1), 251–256 (2011)
42. J.I. Langford, A. Wilson, Scherrer after sixty years: a survey and some new results in the determination of crystallite size. J. Appl. Crystallogr. **11**(2), 102–113 (1978)
43. J.I. Langford, A rapid method for analysing the breadths of diffraction and spectral lines using the Voigt function. J. Appl. Crystallogr. **11**(1), 10–14 (1978)
44. L.E. Brus, Electron–electron and electron-hole interactions in small semiconductor crystallites: The size dependence of the lowest excited electronic state. J. Chem. Phys. **80**(9), 4403–4409 (1984)
45. E.M. Wong, P.G. Hoertz, C.J. Liang, B.-M. Shi, G.J. Meyer, P.C. Searson, Influence of organic capping ligands on the growth kinetics of ZnO nanoparticles. Langmuir **17**(26), 8362–8367 (2001)
46. J. Tauc, Optical properties and electronic structure of amorphous Ge and Si. Mater. Res. Bull. **3**(1), 37–46 (1968)
47. T. Trupke, M. Green, P. Würfel, Improving solar cell efficiencies by down-conversion of high-energy photons. J. Appl. Phys. **92**(3), 1668–1674 (2002)
48. H. Hovel, R. Hodgson, J. Woodall, The effect of fluorescent wavelength shifting on solar cell spectral response. Solar Energy Mater. **2**(1), 19–29 (1979)
49. D. Timmerman, I. Izeddin, P. Stallinga, I. Yassievich, T. Gregorkiewicz, Space-separated quantum cutting with silicon nanocrystals for photovoltaic applications. Nat. Photonics **2**(2), 105–109 (2008)
50. Z. Yuan et al., Silicon nanocrystals as a photoluminescence down shifter for solar cells. Sol. Energy Mater. Sol. Cells **95**(4), 1224–1227 (2011)
51. A.B. Or, J. Appelbaum, Dependence of multi-junction solar cells parameters on concentration and temperature. Sol. Energy Mater. Sol. Cells **130**, 234–240 (2014)
52. P. Singh, N.M. Ravindra, Temperature dependence of solar cell performance—an analysis. Sol. Energy Mater. Sol. Cells **101**, 36–45 (2012)
53. O. Dupré, R. Vaillon, M.A. Green, Experimental assessment of temperature coefficient theories for silicon solar cells. IEEE J. Photovolt. **6**(1), 56–60 (2015)
54. S. Chander, A. Purohit, A. Sharma, S. Nehra, M. Dhaka, A study on photovoltaic parameters of mono-crystalline silicon solar cell with cell temperature. Energy Rep. **1**, 104–109 (2015)
55. D.T. Cotfas, P.A. Cotfas, O.M. Machidon, Study of temperature coefficients for parameters of photovoltaic cells. Int. J. Photoenergy (2018). https://doi.org/10.1155/2018/5945602

56. R. Lopez-Delgado, M. Tostado-Plascencia, M.E. Álvarez-Ramos, A. Ayón, Silicon solar cell efficiency improvement employing photoluminescent properties of chlorophyll-A. Microelectron. Eng. **216**, 111047 (2019)
57. M. Chinnasamy, R. Rathanasamy, S. Sivaraj, G. Velu-Kaliyannan, M.S. Anbupalani, S.K. Jaganathan, Influence of ZnSe surface coatings for enhancing the performance of multicrystalline silicon solar cells. J. Electron. Mater. **51**(6), 2833–2842 (2022)
58. R. Chen, Y. Hu, X. Li, J. He, S. Zhang, Silicon quantum dots prepared by electrochemical etching and their application in solar cells. J. Mater. Sci. **34**(13), 1105 (2023)
59. F. Sgrignuoli et al., Modeling of silicon nanocrystals based down-shifter for enhanced silicon solar cell performance. J. Appl. Phys. (2012). https://doi.org/10.1063/1.3679140
60. A. Apostoluk et al., Improvement of the solar cell efficiency by the ZnO nanoparticle layer via the down-shifting effect. Microelectron. Eng. **127**, 51–56 (2014)
61. R. Rothemund, Optical modelling of the external quantum efficiency of solar cells with luminescent down-shifting layers. Sol. Energy Mater. Sol. Cells **120**, 616–621 (2014)
62. E. Klampaftis, D. Ross, K.R. McIntosh, B.S. Richards, Enhancing the performance of solar cells via luminescent down-shifting of the incident spectrum: a review. Sol. Energy Mater. Sol. Cells **93**(8), 1182–1194 (2009)

Publisher's Note Springer Nature remains neutral with regard to jurisdictional claims in published maps and institutional affiliations.

Springer Nature or its licensor (e.g. a society or other partner) holds exclusive rights to this article under a publishing agreement with the author(s) or other rightsholder(s); author self-archiving of the accepted manuscript version of this article is solely governed by the terms of such publishing agreement and applicable law.